Monthly Notices
of the
ROYAL ASTRONOMICAL SOCIETY

MNRAS **479,** L1–L6 (2018)
Advance Access publication 2018 May 14

doi:10.1093/mnrasl/sly085

Anticorrelation between X-ray luminosity and pulsed fraction in the Small Magellanic Cloud pulsar SXP 1323

Jun Yang,[1★] Andreas Zezas,[2] Malcolm J. Coe,[3] Jeremy J. Drake,[2] JaeSub Hong,[2] Silas G. T. Laycock[4] and Daniel R. Wik[1]

[1]*Department of Physics and Astronomy, the University of Utah, Salt Lake City, Utah 84112, USA*
[2]*Harvard-Smithsonian Center for Astrophysics, Cambridge, MA 02138, USA*
[3]*Physics and Astronomy, University of Southampton, Southampton SO17 1BJ, UK*
[4]*Department of Physics and Applied Physics, University of Massachusetts, Lowell, MA 01854, USA*

Accepted 2018 May 8. Received 2018 May 8; in original form 2018 January 3

ABSTRACT

We report the evidence for the anticorrelation between pulsed fraction (PF) and luminosity of the X-ray pulsar SXP 1323, found for the first time in a luminosity range 10^{35}–10^{37} erg s^{-1} from observations spanning 15 yr. The phenomenon of a decrease in X-ray PF when the source flux increases has been observed in our pipeline analysis of other X-ray pulsars in the Small Magellanic Cloud. It is expected that the luminosity under a certain value decreases as the PF decreases due to the propeller effect. Above the propeller region, an anticorrelation between the PF and the flux might occur either as a result of an increase in the unpulsed component of the total emission or a decrease of the pulsed component. Additional modes of accretion may also be possible, such as spherical accretion and a change in emission geometry. At higher mass accretion rates, the accretion disc could also extend closer to the neutron star surface, where a reduced inner radius leads to hotter inner disc emission. These modes of plasma accretion may affect the change in the beam configuration to fan-beam dominant emission.

Key words: pulsars: individual: SXP 1323 – X-rays: binaries.

1 INTRODUCTION

X-ray pulsars comprise two stars, a neutron star (NS, descended from a star with initial mass > 8 M$_\odot$; Verbunt & van den Heuvel 1995), and a mass-losing companion star, also of large mass. The general picture of accretion on to X-ray pulsars consists of a flow in a wind or disc to the magnetosphere and then along the dipole field lines on to the magnetic poles of the NS. The pulsed fraction (PF), i.e. the relative amplitude of the emerging pulse profile, bears key information on the relation between X-ray emission from the accretion column (pulsed emission) and other regions of the accretion flow or NS surface (unpulsed emission), e.g. Beloborodov (2002).

The Small Magellanic Cloud (SMC) pulsar SXP 5.05 was reported by Coe, Bartlett & Bird (2015) to show a positive correlation between the PF and luminosity, as shown in their fig. 11. Those data were taken while SXP 5.05 was undergoing high levels of accretion. At low-mass accretion rates, Cui (1997) reported two X-ray pulsars (GX 1+4 and GRO J1744−28) whose PF decreases as the X-ray flux drops below a certain threshold. This is an indication of the propeller effect (Illarionov & Sunyaev 1975) that takes place when the pulsar magnetosphere grows beyond the co-rotation radius, and the centrifugal force prevents accreting matter from reaching the magnetic poles.

Tiengo, Mereghetti & Turolla (2005) observed an anticorrelation between PF and the corresponding flux of 1E 1048.1−5937 in the Milky Way. Spectral variations as a function of the pulse phase shows the hardest spectrum at pulse maximum. Lutovinov & Tsygankov (2009) presented marginal evidence for an anticorrelation of PF and energy in source 4U 0115+63 and Her X-1. Fig. 4 from Tsygankov et al. (2007) shows the increase of energy in 4U 0115+63 is not uniform but has local maximum near the cyclotron line. A positive and an anticorrelation is observed at low and high energy, respectively.

Tsygankov, Lutovinov & Serber (2010) noted the PF of V 0332+53 increases with decreasing photon energy below 12–15 keV, which is difficult to explain. An anti and a positive correlation is observed at low and high luminosities, respectively (see their fig. 10). Below $\sim 10^{38}$ erg s^{-1} the anticorrelation is in accordance with a geometry model in which the PF is determined by the luminosity-dependent visible areas of the accretion columns. However, in the photon energy range 25–45 keV the observed correlation does not fully conform to the model. Parmar, White & Stella (1989) applied a geometric model to describe the pulse shape of X-ray pulsar EXO 2030+375 and showed that below a luminosity of 4×10^{36} erg s^{-1}, the pencil beam becomes dominant compared

★ E-mail: junyang@astro.utah.edu

to the fan-beam, along with an increase in the unpulsed component and a decrease in the luminosity. In Beloborodov (2002)'s classes of pulse profiles, visibility of the two polar caps depends on the angle between the magnetic rotation axis and dipole axis. If both poles are continuously visible, it is possible to have no pulsations. As shown in the modelled light curves of fig. 5 from Yang et al. (2017b), in classes 2 and 4 of the upper panel, and classes 3 and 4 of the middle panel, when both hot spots are visible, the observed pulse shows a plateau.

We have collected and analysed the comprehensive archive of *XMM–Newton* (116), *Chandra* Advanced CCD Imaging Spectrometer (ACIS-I) (151), and *RXTE* (952) observations of the known pulsars in the SMC, spanning the years 1997–2014. Our pipeline generates a suite of products for each pulsar detection: spin period, flux, event list, high-time resolution light-curve, pulse-profile, periodogram, and spectrum. Combining all three satellites, we generated complete histories of the spin periods, pulse amplitudes, pulsed fractions, and X-ray luminosities (Yang et al. 2017a). Based on this archive, the relationship between the PF and luminosity of the SMC pulsars have drawn our attention. We find a surprising anticorrelation between PF and luminosity in SMC X-ray pulsars, for example, SXP 1323, SXP 893, SXP 756, SXP 726, SXP 701, SXP 348, and SXP 323. In this work, we show an example (SXP 1323) of this phenomenon and discuss the mechanism behind these results. We selected this source because it has the most data points compared to the other pulsars with anticorrelations.

SXP 1323 (a.k.a. RX J0103.6-7201) was discovered by Haberl & Pietsch (2005) and shows one of the longest pulse periods known in the SMC. The names of the optical companion star are [MA93] 1393 (Meyssonnier & Azzopardi 1993) and [M2002] SMC 56901 (Massey 2002). Carpano et al (2017) found the orbital period of this Be/X-ray binary (BeXB) to be 26.2 d, which is very short for such a long spin period pulsar. It is located at RA = 01:03:37.5 and Dec. = −72:01:33 with a positional uncertainty of 1.1 arcsec (Lin, Webb & Barret 2012). The spectral type of this X-ray binary counterpart is B0 with a luminosity class of III–V (McBride et al. 2008).

In this paper, we present the pulsed fraction dependence on luminosity from 15 yr of X-ray monitoring for SXP 1323. We aim to have a deeper understanding of the accretion process under the anticorrelation of the PFs and luminosities.

2 OBSERVATIONS AND METHODS

Yang et al. (2017a) have collected and analysed 36 *XMM–Newton* and 108 *Chandra* X-ray observations up until 2014 for SXP 1323. *XMM–Newton* has detected this source 36 times and in 10 of these observations its pulsations are found. As for *Chandra*, we only used the ACIS-I detections: 63 out of 108 observations yield source detections and 14 observations have detected its pulsations. We are not including *RXTE* observations in this analysis since *RXTE* does not provide the required PF information. The *RXTE* Proportional Counter Array is a non-imaging detector and multiple sources are always in the field of view, so the unpulsed component cannot be reliably measured.

The observations we used for SXP 1323 with pulsations detected are shown in Table 1. The pulsations are with a significance of $s \geq 99$ per cent according to equation 2 of Yang et al. (2017a).

In order to test the correlation with luminosities and make the results convincible, three different definitions of PF were calculated by integrating over the pulse profile. The simplified formulas are shown in equations (1)–(3).

Table 1. The *XMM–Newton* and *Chandra* ACIS-I X-ray observations in which the pulsations for SXP 1323 have been detected. The first column is the observation ID, the second and third columns show observing Modified Julian Date (MJD) and source flux, and the last two columns are the photon counts (for xmm, it is the medium value from the three EPIC instruments) and exposure time.

XMM–Newton ID	MJD	Flux (erg s^{-1} cm^{-2})	Photon counts	Exposure time (ks)
135 722 401	53292.38	7.32×10^{-13}	458	31.11
123 110 301	51651.15	1.50×10^{-12}	2020	21.66
135 722 701	53845.10	4.29×10^{-12}	5096	30.48
135 720 801	52268.75	2.10×10^{-12}	2190	35.02
135 721 701	52959.26	1.41×10^{-12}	3752	27.36
135 722 501	53477.93	4.69×10^{-12}	9129	37.12
412 980 201	54215.52	2.50×10^{-12}	2407	36.42
135 721 901	53123.30	3.21×10^{-13}	1251	35.23
412 980 501	54575.39	3.44×10^{-12}	3383	29.92
412 980 301	54399.41	1.80×10^{-12}	2725	37.12
Chandra ID	–	–	–	–
1533	52065.27	2.33×10^{-12}	984	7.42
1536	52065.57	2.04×10^{-12}	860	7.42
1542	52065.76	1.69×10^{-12}	699	7.42
1786	51728.55	1.66×10^{-12}	738	7.58
2841	52249.09	1.62×10^{-12}	686	7.46
6050	53352.15	8.25×10^{-13}	336	7.16
6052	53353.37	8.96×10^{-13}	358	7.54
6056	53356.31	5.064×10^{-13}	253	8.01
6060	53534.55	9.00×10^{-13}	1033	19.8
6749	53816.60	1.61×10^{-12}	1830	19.51
6757	53891.55	5.24×10^{-13}	582	19.8
8361	54136.10	1.14×10^{-12}	1283	19.79
8364	54142.57	4.71×10^{-13}	253	8.45
9693	54501.17	1.55×10^{-12}	657	7.68

$$\mathrm{PF_A} = \frac{f_{\max} - f_{\min}}{f_{\max}}, \tag{1}$$

here $f_{\max}$ is the maximum photon count rate in the pulse profile and $f_{\min}$ is the minimum value as demonstrated in an example of the pulsed profile in Fig. 1. $\mathrm{PF_A}$ is also usually called modulation amplitude.

$$\mathrm{PF_B} = \frac{f_{\mathrm{mean}} - f_{\min}}{f_{\mathrm{mean}}}, \tag{2}$$

f_{mean} is the average flux.

$$\mathrm{PF_S} = \frac{\sqrt{2} f_{\mathrm{rms}}}{f_{\mathrm{mean}}}, \left(\text{and } f_{\mathrm{rms}} = \frac{\sqrt{\sum_i^N (f_i - f_{\mathrm{mean}})^2}}{N} \right), \tag{3}$$

where f_{rms} is the root mean square (rms) flux, N is the number of bins for each folded light curve, and f_i is the mean photon count rate in each bin. For a sinusoid wave, which is a good approximation to most accretion pulsars, the peak-to-peak pulsed flux $f_{\mathrm{pulsed}} = f_{\mathrm{mean}} - f_{\min} = \sqrt{2} f_{\mathrm{rms}}$; for a square wave $f_{\mathrm{pulsed}} = f_{\mathrm{rms}}$ (Bildsten, Chakrabarty & Chiu 1997).

The error of the PF is calculated as following. First get the error of the flux in each bin of the light curve,

$$\mathrm{error}_i = \frac{\sqrt{\sum_j^n (f_i - F_j)^2}}{n}, \tag{4}$$

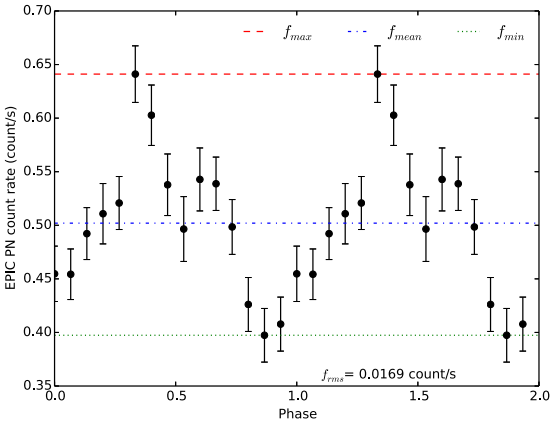

Figure 1. An example of pulse profile for SXP 1323 shows the values used for the PF calculation in equations (1)–(3), and $f_{\rm rms}$ is the root mean square flux. It is an *XMM–Newton* Observation (ID 135 722 701), observed on 2006 April 20.

where F_j is the flux in the ith bin. n is the number of points in each bin. Then we could get the error of $f_{\rm max}$ (error$_{\rm max}$) as well as the error from $f_{\rm min}$ (error$_{\rm min}$). The error of PF$_{\rm A}$ is

$$\text{error}_{\rm PFA} = \sqrt{\frac{\text{error}_{\rm max}^2 + \text{error}_{\rm min}^2}{(f_{\rm max} - f_{\rm min})^2} + \left(\frac{\text{error}_{\rm max}}{f_{\rm max}}\right)^2} \times \text{PF}_{\rm A} \quad (5)$$

In order to calculate error$_{\rm PFB}$ and error$_{\rm PFS}$, first calculate the error of the pulsed flux:

$$e_{\rm pulse} = \frac{\sum_i^N \sqrt{\text{error}_{\rm max}^2 + \text{error}_i^2}}{N}, \quad (6)$$

$$\text{error}_{\rm PFB} = \frac{e_{\rm pulse}}{f_{\rm mean}}; \quad (7)$$

$$\text{error}_{\rm PFS} = \sqrt{2}\frac{e_{\rm pulse}}{f_{\rm mean}} \times \text{PF}_{\rm S}. \quad (8)$$

Note, in Yang et al. (2017a) the pulsed fraction from *XMM–Newton* is PF$_{\rm B}$ and the ones from *Chandra* are PF$_{\rm A}$. Here we used PF$_{\rm A}$ and PF$_{\rm B}$ for both *XMM–Newton* and *Chandra* observations.

PF$_{\rm A}$ has intuitive appeal, but it is more difficult to determine the $f_{\rm min}$ than $f_{\rm mean}$ (Bildsten et al. 1997). People generally use PF$_{\rm A}$ for light curves from long time exposures, where signal-to-noise ratio is large. PF$_{\rm B}$ is smaller than PF$_{\rm A}$, but more stable as $f_{\rm mean}$ is easier to be determined than $f_{\rm max}$. PF$_{\rm S}$ is used for relatively short time exposure.

The PF as a function of luminosity for SXP 1323 is shown in Fig. 2. Although the light curves were extracted from the higher time resolution EPIC-PN data (Yang et al. 2017a), the luminosities used in Fig. 2 were obtained from the total *XMM–Newton* flux available in the three *XMM–Newton* catalogues since they are more complete than the instrument-specific fluxes. These fluxes are based on a spectral model of a power law of slope 1.7 absorbed by a Hydrogen column of 3×10^{20} cm^{-2} (0.2–12 keV).[1]

The trend between PF$_{\rm A}$ and luminosity is

$$\text{PF}_{\rm A} = -0.399 \log\left(\frac{L_{\rm X}}{10^{35}\ \text{erg s}^{-1}}\right) + 0.850, \quad (9)$$

[1] https://www.cosmos.esa.int/web/xmm–Newton/uls-userguide

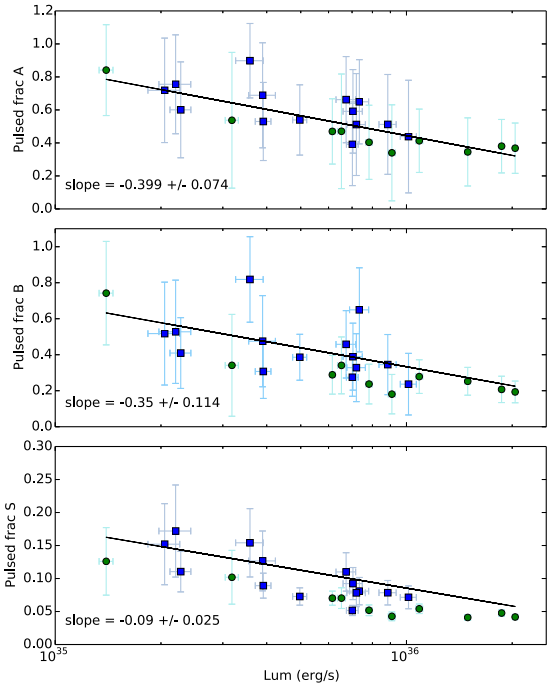

Figure 2. The PF as the function of luminosity for SXP 1323. Green circles are the *XMM–Newton* detections and blue square symbols present *Chandra* observations. The three panels show the PFs with different calculations which are in equations (1)–(3).

The fit between PF$_{\rm B}$ and luminosity is

$$\text{PF}_{\rm B} = -0.350 \log\left(\frac{L_{\rm X}}{10^{35}\ \text{erg s}^{-1}}\right) + 0.669. \quad (10)$$

The anticorrelation of PF$_{\rm S}$ and luminosity is fitted as

$$\text{PF}_{\rm S} = -0.101 \log\left(\frac{L_{\rm X}}{10^{35}\ \text{erg s}^{-1}}\right) + 0.173, \quad (11)$$

where $L_{\rm X}$ is in erg s^{-1}.

The trend with PF$_{\rm A}$ is steeper than the one with PF$_{\rm B}$, and even more steeper than PF$_{\rm S}$. PF$_{\rm A}$ is the most popular way to show the pulsed fraction of the X-ray pulse profiles, therefore, the linear regression is more convincing. However, all of them show the similar anticorrelation.

Monte Carlo simulations are performed to estimate the false-positive detection rate for the correlation between these two observables, from which the significance level is estimated.

For the correlation in each panel of Fig. 2, 4000 trial generates 4000 simulated data. Based on these data, the fitting is performed. One of the fitting parameters (slope) is shown in the histograms of Fig. 3. We interpret positive slopes as false positive detections of an anticorrelation in the real data. The number of false positives from Fig. 3 corresponds to a probability of 95.43, 93.28, and 92.68, for the anticorrelation found by using PF$_{\rm A}$, PF$_{\rm B}$, and PF$_{\rm S}$, respectively. Therefore, the fit of the correlations in Fig. 2 is around $\sim 2\sigma$ confidence.

3 THEORETICAL MECHANISMS

Mukerjee, Agrawal & Paul (2000) observed a decrease in the pulsed fraction with decreasing luminosity of the X-ray pulsar Cepheus X-4 (GS 2138+56). However, they argued that the decrease in the pulsed fraction, depending on the accretion flow geometry with respect to

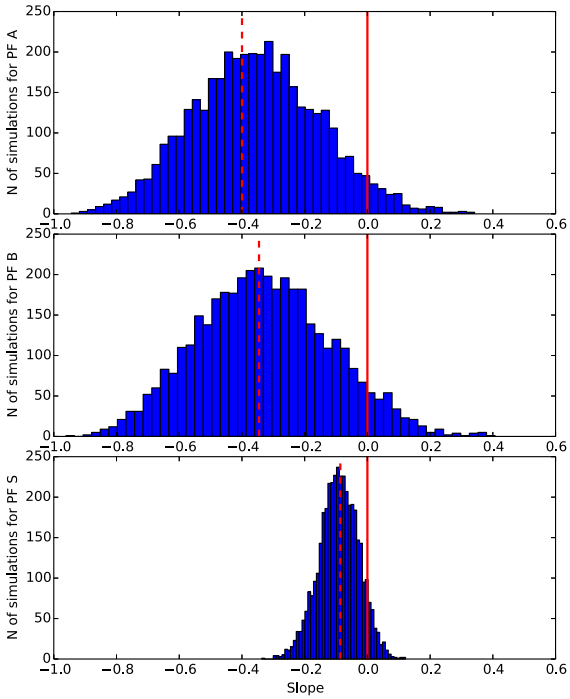

Figure 3. Frequency distribution of correlation slopes for PF_A (upper), PF_B (middle), and PF_S (bottom) obtained using Monte Carlo method with 4000 simulations. The heights of bars indicate the number of parameter values in the equally spaced bins. The limit for false positive detections of an anticorrelation is shown as red solid lines at slope 0.0. The dashed lines are the slopes from Fig. 2.

line of sight, is not a consequence of propeller effect. They propose as a more likely scenario a different mode of accretion occurring below a certain luminosity. These additional entry modes of plasma may affect the emission geometry to be more fan-beam-like pattern, which will increase the unpulsed flux, and the pulsed fractions end up being smaller.

However, for SXP 1323, the PF increases as the luminosity decreases. The critical luminosity mentioned in Mukerjee et al. (2000) is the maximum luminosity $L_X(\mathrm{min})$ at which the centrifugal inhibition dominates, resulting in the propeller effect (e.g. Shtykovskiy & Gilfanov 2005; Tsygankov et al. 2016; Christodoulou et al. 2016):

$$L_X(\mathrm{min}) = 2\times10^{37}\left(\frac{R}{10^6\,\mathrm{cm}}\right)^{-1}\left(\frac{M}{1.4\,\mathrm{M}_\odot}\right)^{-\frac{2}{3}} \times\left(\frac{\mu}{10^{30}\,\mathrm{G\,cm^3}}\right)^{2}\left(\frac{P_s}{1\mathrm{s}}\right)^{-\frac{7}{3}}\mathrm{erg\,s^{-1}}, \quad (12)$$

where R, M, μ, and P_s are the radius, mass, magnetic moment, and spin period of the NS, respectively.

We use a surface polar magnetic field strength $B = 2.6\times10^{12}$ G (Mihara et al. 1991) and $R = 10$ km, for a dipole-like field configuration, $\mu = B\times R^3 = 2.6\times10^{30}\,\mathrm{G\,cm^3}$. Assuming $M = 1.4\mathrm{M}_\odot$, we calculate the minimum luminosity below which the propeller effect will occur in SXP 1323 to be $L_X(\mathrm{min}) = 7.03\times10^{30}\,\mathrm{erg\,s^{-1}}$. In our analysis, all of the luminosities observed are higher than this critical value, therefore it is highly unlikely that the anticorrelation is the result of the propeller effect.

We can see the PF drops quickly as the luminosity increases up to $\sim10^{36}\,\mathrm{erg\,s^{-1}}$. This is consistent with Campana, Gastaldello & Stella (2001)'s result above a certain critical luminosity of $\sim10^{35}\,\mathrm{erg\,s^{-1}}$ in the X-ray pulsar 4U 0115+63 in our Galaxy. Campana et al. (2001) expressed the source accretion luminosity as two components: the luminosity of the disc extending down to the magnetospheric boundary, L_{disc}; and the luminosity released within the magnetosphere L_{mag} by the mass inflow rate that accretes on to the NS surface. They claimed that the pulsed fraction is expected to remain unaltered as long as L_{mag} dominates, while L_{disc} is expected to be unpulsed, resulting in a decreasing pulsed fraction as its luminosity increases. It explains the PF trend only at the luminosities larger than $\sim10^{35}\,\mathrm{erg\,s^{-1}}$ in fig. 2 of Campana et al. (2001).

Assuming that there are two X-ray components: the accretion column (L_{col}) and the accretion disc (L_{disc}), the luminosity of the accretion column should be relatively stable since it would be locally Eddington, and the luminosity of the disc changes because at high-mass accretion rate ($\dot{M}$) the magnetospheric radius (R_{mag}) gets smaller and the L_{disc} increases.

From the relation between R_{mag} and $\dot{M}$ (for a given P_s and magnetic field B) and feeding this through a standard Shakura–Sunyaev disc, we have that

$$T_{\mathrm{disc}} \propto \left\{\frac{\dot{M}}{R^3}\left[1-\left(\frac{R_{\mathrm{mag}}}{R}\right)^{\frac{1}{2}}\right]\right\}^{\frac{1}{4}}, \quad (13)$$

$$L_{\mathrm{disc}} \propto T_{\mathrm{disc}}^4\times R^2 \simeq \dot{M}\times R^{\frac{5}{4}}, \quad (14)$$

where T_{disk} is the temperature. If luminosity from the accretion column L_{col} is constant, R_{mag} decreases and L_{disc} increases. The predicted PF should change with increasing luminosity due to the unpulsed disc emission.

Our anticorrelation is still at odds with the trend reported for many other pulsars in the literature (e.g. Mukerjee et al. 2000; Coe et al. 2015). The possible reason is that the spin period matters, as the pulsars in Mukerjee et al. (2000) and Coe et al. (2015) have short spin periods of 66.27 and 5.05 s, respectively. It could be that the PF changes of the short period pulsars depend on their luminosities.

In the following, we discuss the PF luminosity anticorrelation in the context of different models for X-ray emission in accreting pulsars.

3.1 Spherical accretion

The flow of material towards the pulsar might not take place through an accretion disc but instead via a spherical accretion flow, a natural consequence of wind-fed accretion, as opposed to Roche lobe overflow. The spherical accretion should be outside the accretion column and would obscure it (unless highly ionized). Also at low luminosity, the magnetospheric radius should be large enough to truncate the accretion flow. This accretion model was applied to black holes by Nobili, Turolla & Zampieri (1991). The accretion of gas on to the compact object can be a very efficient way of converting gravitational potential energy into radiation. Traditional spherical accretion is thought of as a good approximation for isolated compact objects. Ikhsanov, Pustil'nik & Beskrovnaya (2005) has applied the spherical accretion model to High-Mass X-ray binaries (HMXBs), especially the long spin period pulsars. Zeldovich and Shakura (1969) presented a model to describe the gravitational energy of matter accreted on to an NS and released in a thin layer above the surface. Variations of this idea have also been applied in detailed models (e.g. Turolla et al. 1994, for spherical accretion). The deep layers of the NS atmosphere are heated by the outer layer and produce soft thermal photons (Cui et al. 1998). The hard X-ray photons are from the polar hot spots, which contribute to the

pulsed flux observed. The soft X-ray photons from spherical accretion would mainly contribute to the unpulsed component of flux. Spherical accretion becomes more prominent as the luminosity and mass accretion rate increases, which leads to a smaller PF.

3.2 NS whole surface thermal emission

Generally, there are two components of the X-ray emission from NSs: thermal emission and non-thermal emission. The non-thermal emission is caused by pulsar radiation in the magnetosphere and its own rotation activity, which is suppressed when accreting. Thermal emission is from the whole surface of a cooling NS and/or from the small hot spots around the magnetic poles on the star surface (Becker 2009). It is also heated by accretion. The thermal radiation from the entire stellar surface can dominate at soft X-ray energies for middle-aged pulsars (∼100 kyr) and younger pulsars (∼10 kyr).

If thermal emission is a significant component of the X-rays from SXP 1323 and this component increases, it would represent and increase in unpulsed flux such that the PF becomes smaller.

3.3 Change in emission geometry

Ghosh & Lamb (1979) found $\dot{P} \propto L_X^{6/7}$ assuming the effective inertial moment of the NS is constant, so a higher accretion rate and L_X could cause the observed high spin-up rate of this pulsar. The accreted mass interacts with the magnetosphere, and the accretion disc extends inward to some equilibrium radial distance above the NS's surface (Malina & Bowyer 1991). Yang et al. (2017a) has reported this pulsar's average spin-up rate as 6 ± 3 ms d^{-1} based on data from three X-ray satellites from 1997–2014. Carpano et al (2017) has presented an even faster spin-up of ∼59.3 ms d^{-1} based on recent observations from 2006 to 2016. The higher spin period and mass accretion rate could build up a higher accretion column above the polar caps. As the height of the accretion column increases, scattering of photons off in-falling electrons gets more prominent. This increases the fraction of emission escaping the column to the side, i.e. a fan-beam emerges (e.g. Becker, Klochkov & Schönherr 2012). Fan-beam emission becomes dominant, which reduces the eclipse of the accretion column. Furthermore, the contribution of the flux reflected by the NS surface is significant (Mushtukov, Verhagen & Tsygankov 2018). It raises the unpulsed flux, therefore we see the luminosity increasing and the pulsed fraction decreasing.

Romanova, Kulkarni & Lovelace (2008) used 3D magnetohydrodynamic simulations for a star that might be in the stable or unstable regime of accretion. In the unstable regime, matter penetrates into the magnetosphere and is deposited at random places on the surface of the star, which made the pulsations intermittent or with no pulsations. Therefore, the PF is reduced when the overall X-ray flux increases which may be also due to the transition to the unstable accretion regime.

In this scenario, we predict that the slope of the PF versus the luminosity will decrease as the spin periods of the pulsars increase. We will further investigate all of the pulsars in our current library to test this prediction.

4 CONCLUSIONS

The anticorrelation between the PF and luminosity in SXP 1323 reveals that different accretion modes are possible. This could be related to the puzzle of the existence of long period pulsars which are hard to explain (Ikhsanov, Beskrovnaya & Likh 2014) without invoking non-standard accretion modes (such as spherical accretion). However, the significance of the anticorrelation is not high enough to prove its existence. SXP 1323 is the best example within our sample and more high quality data from the future observations are still needed to check up on the anticorrelation.

ACKNOWLEDGEMENTS

We would like to thank the anonymous referee whose valuable suggestions and comments have significantly improved the quality of the paper.

REFERENCES

Becker P. A. et al., 2012, A&A, 544, A123
Becker W., 2009 , Neutron Stars and Pulsars, Astrophysics and *S*pace Science Library, Vol. 357, Springer, Berlin, p. 182
Beloborodov A. M., 2002, ApJ, 566, 85
Bildsten L. et al., 1997, ApJS, 113, 367
Campana S., Gastaldello F., Stella L., Israel G. L., Colpi M., Pizzolato E., Orlandini M., Dal Fiume D., 2001, ApJ, 561, 924
Carpano S., Haberl F., Sturm R., 2017, A&A, 602, A81
Christodoulou D. M., Laycock S. G. T., Yang J., Fingerman S., 2016, ApJ, 829:30
Coe M. J., Bartlett E. S., Bird A. J., Haberl F., Kennea J. A., McBride V. A. , Townsend L. J. , Udalski A., 2015, MNRAS, 447, 2387
Cui W., 1997, ApJ, 482, L163
Cui W., Morgan E. H., Titarchuk L. G., 1998, ApJ, 504, L27
Ferrigno C., Segreto A., Santangelo A., Wilms J., Kreykenbohm J., Denis M., Staubert R., 2007, A&A, 462, 995
Ghosh P., Lamb F. K., 1979, ApJ, 234, 296
Haberl F., Pietsch W., 2005, A&A, 438, 211
Ikhsanov N., Beskrovnaya N., Likh Y., 2014, Int. J. Mod. Phys. Conf. Ser. 28, 1460187
Ikhsanov N. R., Pustil'nik L. A., Beskrovnaya N. G., 2012, in Sulem P., and Mond M., AIP Conf. Proc. Vol. 1439, A new look at spherical accretion in high mass X-ray binaries. Am. Inst. Phys., New York, 237–248
Illarionov A. F., Sunyaev R. A., 1975, A&A, 39, 185
Lin D., Webb N. A., Barret D., 2012, ApJ, 756, 27
Lutovinov A. A., Tsygankov S. S., 2009, Astron. Lett., 35, 433
Malina R. F., Bowyer S., 1991, Extreme Ultraviolet Astrnomy, , Pergamon Press, New York, p. 222
Massey P., 2002, ApJS, 141, 81
McBride V. A., Coe M. J., Negueruela I., Schurch M. P. E., McGowan K. E., 2008, MNRAS, 388, 1198
Meyssonnier N., Azzopardi M., 1993, A&AS, 102, 451
Mihara T., Makishima K., Kamijo S., Ohashi T., 1991, ApJ, 379, L61
Mukerjee K., Agrawal P. C., Paul B., Rao A. R., Seetha S., Kasturirangan K., 2000, A&A, 353, 239
Mushtukov A. A., Verhagen P. A., Tsygankov S. S., van der Klis M., Lutovinov A. A., Larchenkova T. I., 2018, MNRAS, 474, 5425
Nobili L., Turolla R., Zampieri L., 1991, ApJ, 383, 250
Parmar A. N., White N. E., Stella L., 1989, ApJ, 338, 373
Romanova M. M., Kulkarni A. K., Lovelace R. V. E., 2008, ApJ, 673, L171
Shtykovskiy P., Gilfanov M., 2005. A&A, 431, 597
Tiengo A., Mereghetti S., Turolla R., Zane S., Rea N., Stella L., Israel G. L., 2005, A&A, 437, 997
Tsygankov S. S., Lutovinov A. A., Churazov E. M., Sunyaev R. A., 2007, Astron. Lett., 33, 368
Tsygankov S. S., Lutovinov A. A., Serber A. V., 2010, MNRAS, 401, 1628
Tsygankov S. S., Mushtukov A. A., Suleimanov V. F., Poutanen J., 2016, MNRAS, 457, 1101
Turolla R., Zampieri L., Colpi M., Treves A., 1994, ApJ, 426, L35
Verbunt F., van den Heuvel E. P. J., 1995, in Lewin W. H. G., van Paradijs J., van den Heuvel E. P. J. eds, X-ray Binaries, Cambridge University Press, Cambridge, p. 457

Yang J., Laycock S. G. T., Christodoulou D. M., Fingerman S., Coe M. J., Drake J. J., 2017a, ApJ, 839, 119
Yang J., Laycock S. G. T., Drake J. J., et al., 2017b, Astron. Nachr./AN., 2015, 44
Zeldovich, Ya. B., Shakura N. I., 1969, AZh, 46, 225 (English transl. in Soviet Astron. 13, 175)

This paper has been typeset from a TEX/LATEX file prepared by the author.